Journal of Biomechanics 95 (2019) 109314

Contents lists available at ScienceDirect

Journal of Biomechanics

journal homepage: www.elsevier.com/locate/jbiomech
www.JBiomech.com

Mechanical characterization of the key portions in locust semi-lunar processes under different strain rates

Chao Wan [a,b,*], Zhixiu Hao [c], Xi-Qiao Feng [a,c]

[a] Institute of Biomechanics and Medical Engineering, Department of Engineering Mechanics, Tsinghua University, Beijing 100084, China
[b] Department of Mechanics, School of Aerospace Engineering, Beijing Institute of Technology, Beijing 100081, China
[c] State Key Laboratory of Tribology, Tsinghua University, Beijing 100084, China

ARTICLE INFO

Article history:
Accepted 6 August 2019

Keywords:
Mechanical property
Energy dissipation
Strain rate
Semi-lunar process
Locust
Nanoindentation

ABSTRACT

The excellent rapid jumping and kicking of locusts are largely attributed to the power amplification mechanisms due to the semi-lunar processes (SLP) at their distal metathoracic femurs, especially dorsal-core (i.e., portion II) and ventral-core parts (i.e., portion III). The physiological range of strain rates at the two portions of locust SLP is quite broad in the periods of energy storage and release (approximately three orders). However, it still remains elusive how the mechanical properties of the two SLP portions change with the strain rate. We identified the elastic moduli and material compositions of SLP portions II and III by using nanoindentation and confocal laser scanning microscope. Apparent and creep-corrected reduced elastic moduli were calculated to represent the total energy absorption and storage, respectively. The results revealed that both portions II and III exhibit strain rate-sensitive elastic moduli, regardless of water content. The efficiency of elastic energy storage is only 51–70% in the case of low strain rate. This work can deepen our understanding in the energy storage and release mechanisms in locust locomotion and further provide guidelines for biomimetic design of power amplification apparatus in jumping robots.

1. Introduction

Cuticle widely exists in the exoskeletons of insects and other arthropods, e.g., their mouthparts, body shells, wing membranes, legs, antennae and setae (Dirks et al., 2013; Zhao et al., 2016). The different exoskeleton parts have diverse mechanical behaviors, which are highly dependent on their composition and microstructure. Variable combinations of composition and microstructure make the exoskeleton optimal to their specific functions. For example, the gradient material distributions in adhesive tarsal setae of ladybird beetles play a key role in their effective adhesion behavior (Peisker et al., 2013), the resilin-dominant endocuticle layered structure endows dragonfly wing veins with higher damping capacity (Rajabi et al., 2016), and the Bouligand pattern in the hierarchical structures of crab exoskeleton renders a high hardness (Chen et al., 2008).

For many insects, rapid locomotion is critical for their survival in nature, which is generally realized by the power amplification mechanisms of legs to provide much higher power output than that can be achieved by muscles alone (Patek et al., 2011). For example, locusts use semi-lunar processes (SLP) as a power amplifier to achieve extraordinary movements like jumping and kicking (Bennet-Clark, 1975; Wan et al., 2016). SLP is a highly-sclerotized banana-shaped cuticle at the distal end of the metathoracic femur, consisting of hard cuticle outside and resilin proteins inside (Bennet-Clark, 1975; Burrows and Sutton, 2012). Our previous study (Wan et al., 2016) revealed that an adult SLP has five portions with different microstructures, compositions and static mechanical properties while the elastic strain energy during jumping and kicking is mainly stored in its dorsal-core and ventral-core parts, i.e., portions II and III (Fig. 1). To store elastic strain energy for the jumping of a locust, its joint pivots shift ventral-proximally, leading to deformation in the SLPs. Most of the elastic strain energy is stored in portion III. Before the kicking of a locust that needs more energy storage, the joint pivots move with larger ventral-proximal shifts and thus the SLPs distort more greatly. In this course, the distal-core part of the SLPs (i.e., portion II) undergoes larger deformations and stores more elastic strain energy.

Moreover, the durations of energy storage and release for jumping and kicking vary from a few milliseconds to one thousand milliseconds: the SLP is bent in 150–800 ms (jumping) or 200–1000 ms (kicking) to store elastic strain energy before the

* Corresponding author at: Department of Mechanics, School of Aerospace Engineering, Beijing Institute of Technology, Beijing 100081, China.
E-mail address: chaowan@bit.edu.cn (C. Wan).

https://doi.org/10.1016/j.jbiomech.2019.08.008
0021-9290/

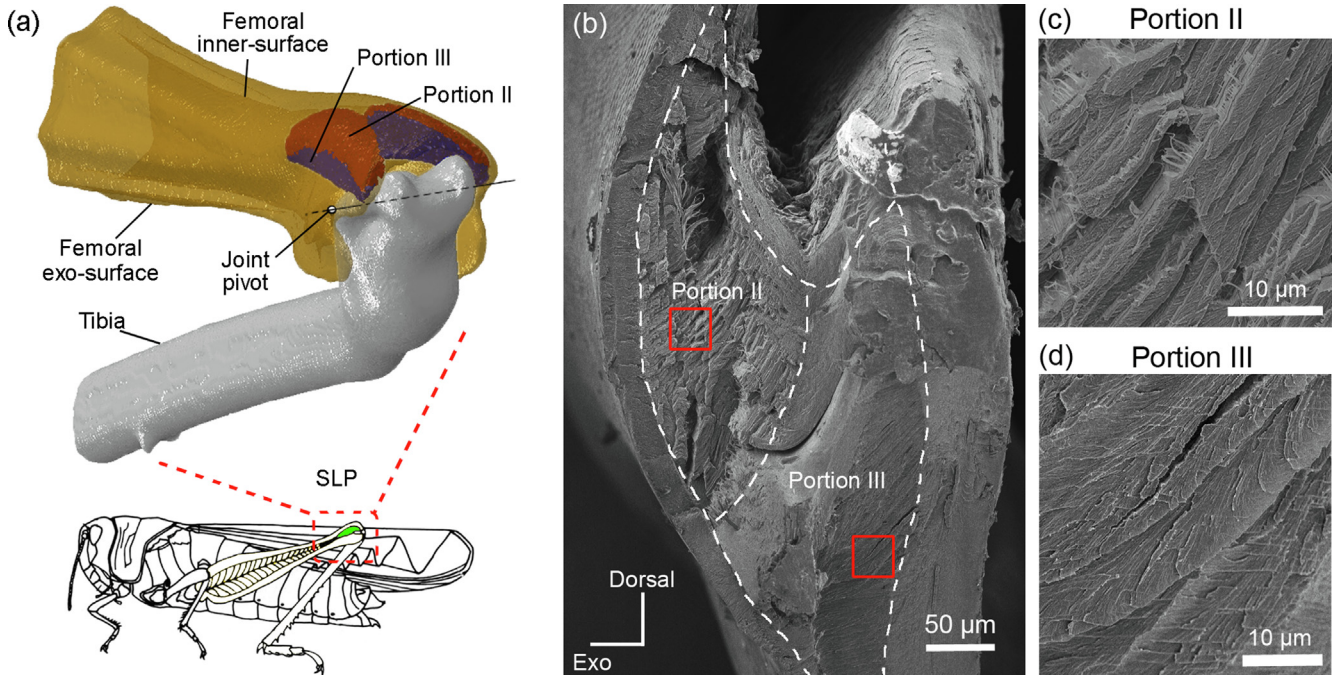

Fig. 1. Anatomical site and microstructure of semi-lunar process (SLP) in an adult locust. (a) The SLP is marked by green color in the whole insect body where its portions II and III are shown in a 3D model of the metathoracic joint. The femur is set as transparent for a clear display of the portions inside. (b) The cross section at the middle site of one unilateral SLP shows the different microstructures between the portions II and III (outlines indicated by dash line). Their detailed images are obtained by magnifying at the red frames, shown in (c) and (d), respectively. (For interpretation of the references to color in this figure legend, the reader is referred to the web version of this article.)

movements and then restores to its initial configuration in a very short time (25–30 ms for jumping and around 6 ms for kicking) to release the stored energy (Bennet-Clark, 1975; Burrows and Morris, 2001). The range of strain rates in the SLP is broad and can vary by three orders for storing and releasing energy. As is well known, the elastic strain energy stored in a material under the same strain condition depends on its elastic modulus. However, it is remain unclear whether and how the elastic modulus of the SLP changes with the strain rate. In this paper, we compare the mechanical properties of the two key SLP portions, II and III, under different strain rates, and their material compositions as well. This study not only deepens our understanding of the energy storage and release mechanisms in locust locomotion, but also contributes to biomimetic design of power amplification in bio-inspired jumping robots.

2. Materials and methods

2.1. Specimen preparation

Twelve metathoracic femurs (including intact SLPs) were excised from twelve adult *Locusta migratoria manilensis* of either sex (at least 2 weeks after their final molt), which were fed in a gregarious population at Jiyuan locust-breeding plant in Anhui Province of China. Six femurs were tested to obtain the mechanical properties of the SLPs while the remaining six femurs were used to identify their material compositions.

2.2. Mechanical properties

The six femurs were dried for 24 h, embedded in light-curing resin (Technovit 7200VLC, EXAKT Inc., Germany), and cross-sectioned at the middle site of the SLP with a diamond band saw (EXAKT 300CP, EXAKT Inc., Germany). The cross-sectional surface was polished by a grinder-polisher with polishing suspension of 0.05 μm (Metaserv 3000, Buehler Inc., Illinois, USA).

Nanoindentations were performed on the cross-section of the SLP portions II and III to identify the mechanical properties along the femoral longitudinal axis. First, the dry SLP samples were tested in ambient air using a nanoindentation instrument with Berkovich diamond indenter (NanoForce, Bruker Corporation, Karlsruhe, Germany). Then all six samples were rewetted by distilled water for 24 h and tested in distilled water using another nanoindentation system with a fluid Berkovich probe (TI 750 ubi, Hysitron Inc., MN, USA). The mechanical properties of the rewetted samples were considered as those of the fresh SLP because it was demonstrated that dry locust cuticles manifest identical mechanical properties to fresh cuticles after rewetted in distilled water for 6 h (Klocke and Schmitz, 2011). The indenting settings for the dry and rewetted samples were the same. The maximum indentation load was 5 mN. A 10 s hold time was dwelled at the peak load to eliminate the effect of material creep (Klocke and Schmitz, 2011). Three loading rates (5, 50, and 500 mN/min) were selected for both the loading and unloading of nanoindentation, corresponding to the strain rates of 0.0083, 0.083, and 0.83 s^{-1}, respectively (Maier et al., 2011). For each strain rate, three indentations were performed at each portion of the SLP samples. Thus, eighteen indentation tests were made for each portion under each strain rate and water condition. To rule out the effects of the portion interfaces and the interference from adjacent indents, all indentation tests were made in the central region of the two portions in each specimen and the spacing between adjacent indents was larger than 20 μm, respectively.

In the nanoindentation tests, the apparent reduced elastic modulus, $E_{r,app}$, was calculated as (Pharr et al., 1992; Oliver and Pharr, 1992; Hay et al., 1999)

$$E_{r,app} = \frac{\sqrt{\pi}}{2\beta}\frac{S_{app}}{\sqrt{A(h_{c,app})}}, \quad (1)$$

$$h_{c,app} = h_{max} - \varepsilon \frac{P_{max}}{S_{app}} \quad (2)$$

where β and ε are the correction coefficients. For the Berkovich indenter, one hasβ = 1.034 andε = 0.75. A is the projected contact area function of the indenter with respect to the contact depth and is calibrated by serial indents on standard fused silica. $h_{c,app}$ is the apparent contact depth. P_{max} and h_{max} are the maximum indenter load and displacement, respectively. The apparent contact stiffness S_{app} was defined as the slope of the initial part of the unloading curve and was usually determined by fitting the upper quarter of the unloading curve (i.e., 75–100%).

To eliminate the material creep effect on the unloading curves, the creep-corrected reduced elastic modulus, $E_{r,cor}$, was defined according to the following modified expressions (Tang and Ngan, 2003; Ngan et al., 2005)

$$E_{r,cor} = \frac{\sqrt{\pi}}{2\beta} \frac{S_{cor}}{\sqrt{A(h_{c,cor})}} \quad (3)$$

$$\frac{1}{S_{cor}} = \frac{1}{S_{app}} + \frac{\dot{h}_h}{|\dot{P}_u|}, \quad (4)$$

$$h_{c,cor} = h_{max} - \varepsilon \frac{P_{max}}{S_{cor}} \quad (5)$$

where S_{cor} is the corrected contact stiffness, $h_{c,cor}$ is the corrected contact depth, $\dot{P}_u$ is the unloading rate of the indenter load, and $\dot{h}_h$ is the tip displacement rate at the end of holding. Since the time–displacement curves within the last 1 s of holding are approximately linear, $\dot{h}_h$ is determined by linear fitting. The typical indentation force–depth curves for the SLP portions II and III under different strain rates and water conditions were shown in the Supplementary Materials.

Using the above method, the $E_{r,app}$ and $E_{r,cor}$ values were calculated for each indentation to represent the total energy absorption and elastic energy storage, respectively. The ratio between these two moduli was defined as $\Re = E_{r,cor}/E_{r,app}$ to identify the efficiency of elastic energy storage under different strain rates.

2.3. Compositional analysis

The other six femurs were cut along the mid-cross section of the SLP using a razor blade, immersed in glycerine (≥99.0%), and mounted on a cover slip with some glycerine around. Given that chitin and resilin in cuticles can be successfully distinguished by different autofluorescences under confocal laser scanning microscope (CLSM) (Michels and Gorb, 2012; Wan et al., 2016), all six samples were observed under a CLSM instrument (Zeiss LSM 710META, Carl Zeiss MicroImaging GmbH, Göttingen, Germany). The measurement settings were the same as those in the literature (Michels and Gorb, 2012; Wan et al., 2016): four pairs of laser excitations and emission filters were used, corresponding to 405 nm and 420–480 nm, 488 nm and ≥490 nm, 555 nm and ≥560 nm, 639 nm and ≥640 nm, respectively. The obtained autofluorescences were shown as blue (emission = 420–480 nm), green (emission ≥490 nm), and red (for both: emission ≥560 nm and ≥640 nm) in the CLSM image after maximum intensity projection. The blue autofluorescence in the CLSM image has been confirmed to be resulted from the resilin by a pH-sensitive test (Details in the Supplementary Materials).

2.4. Statistical analysis

Two-way analyses of variance (ANOVA) with Bonferroni post-hoc were used to compare the nanoindentation results (including $E_{r,cor}$ and $\Re$) of the two dry portions and those of the two rewetted portions under different strain rates. The effects of water content and portion type were analyzed using t-test between the dry and rewetted portions and between portions II and III under the same strain rate, respectively. Paired t-test was used to determine the difference between $E_{r,app}$ and $E_{r,cor}$ for each indentation under the same condition. Significance was defined as $p < 0.05$.

3. Results and discussions

Fig. 2(a) and 2(b) show the nanoindentation results of portions II and III, respectively (details in the Supplementary Materials). It is seen that portion II exhibits a significantly higher $E_{r,cor}$ than portion III under all strain rates, regardless of water content ($P < 0.001$ from t-test). A higher value of $E_{r,cor}$ indicates that more elastic energy can be stored in portion II than that in portion III, as a result from the difference of their microstructure and composition. The CLSM images of SLP (Fig. 2c,d) show deep pink in portion III and red-by-blue layers in portion II, revealing that portion III is a mixture of chitin and resilin while portion II has a higher resilin proportion and some chitin layers. According to our previous study (Wan et al., 2016), portions II and III are composed of regularly- and irregularly-arranged chitin microfibers, respectively (Fig. 1 (b–d)). According to the micromechanics of composites reinforced by aligned fibers, the mechanical properties parallel and perpendicular to the fibrous orientation can be estimated by the models consisting of the matrix and fiber components in series and in parallel, respectively. More specifically, the elastic moduli parallel and perpendicular to the fibrous orientation are expressed as (Chamis, 1989)

$$E^a = R_f E_f^a + R_m E_m = R_f E_f^a + (1 - R_f) E_m \quad (6)$$

$$E^t = \frac{E_m}{1 - \sqrt{R_f}(1 - E_m/E_f^t)} \quad (7)$$

where R_f and $R_m = 1 - R_f$ are the volume fr$E_m$actions of chitin fibers and resilin matrix, respectively, and is the elastic modulus of the resilin matrix. E_f^a and E_f^t are the elastic moduli of chitin fibers along the axial and transverse directions, respectively. For a composite with varying fibrous orientations, the elastic modulus is bounded by the upper and lower limits in Eqs. (6) and (7). It is known that the elastic modulus of chitin fibers is higher by four orders than that of the resilin matrix, i.e., E_m = 1 MPa and $E_f^a = E_f^t$ = 20 GPa (Vincent and Wegst, 2004). The CLSM images of portion II show that the R_m values in portion II is around 30% while that in portion III is assumed to be 10%. Therefore, the femoral longitudinal elastic modulus of portion II is calculated as 14 GPa, whilst portion III has an Young's modulus between 0.019 GPa and 18 GPa (with the mean value being about 9.0 GPa). Though portion II contains more resilin content (soft component) than portion III, the well aligned chitin microfibers in the former yield a higher femoral longitudinal elastic modulus.

In addition, the combination of chitin microfibers and resilin leads to a shortcoming for elastic energy storage and release. The paired t-test analysis shows a significant difference between $E_{r,app}$ and $E_{r,cor}$ under the low strain rate, regardless of the portion and water content ($P < 0.001$). The efficiency ratio of elastic energy storage, $\Re$, under the low rate is distinctly lower than those under the medium and high rates, indicating that a larger amount of work is dissipated by the material due to its viscosity in the case of the low strain rate (listed in Table 1). Specifically, the efficiency ratio $\Re$ under the low strain rate is significantly lower in rewetted portion II than that in rewetted portion III (51 ± 6.8% vs. 69 ± 6.0%). This difference could be attributed to the viscosity of resilin. The large

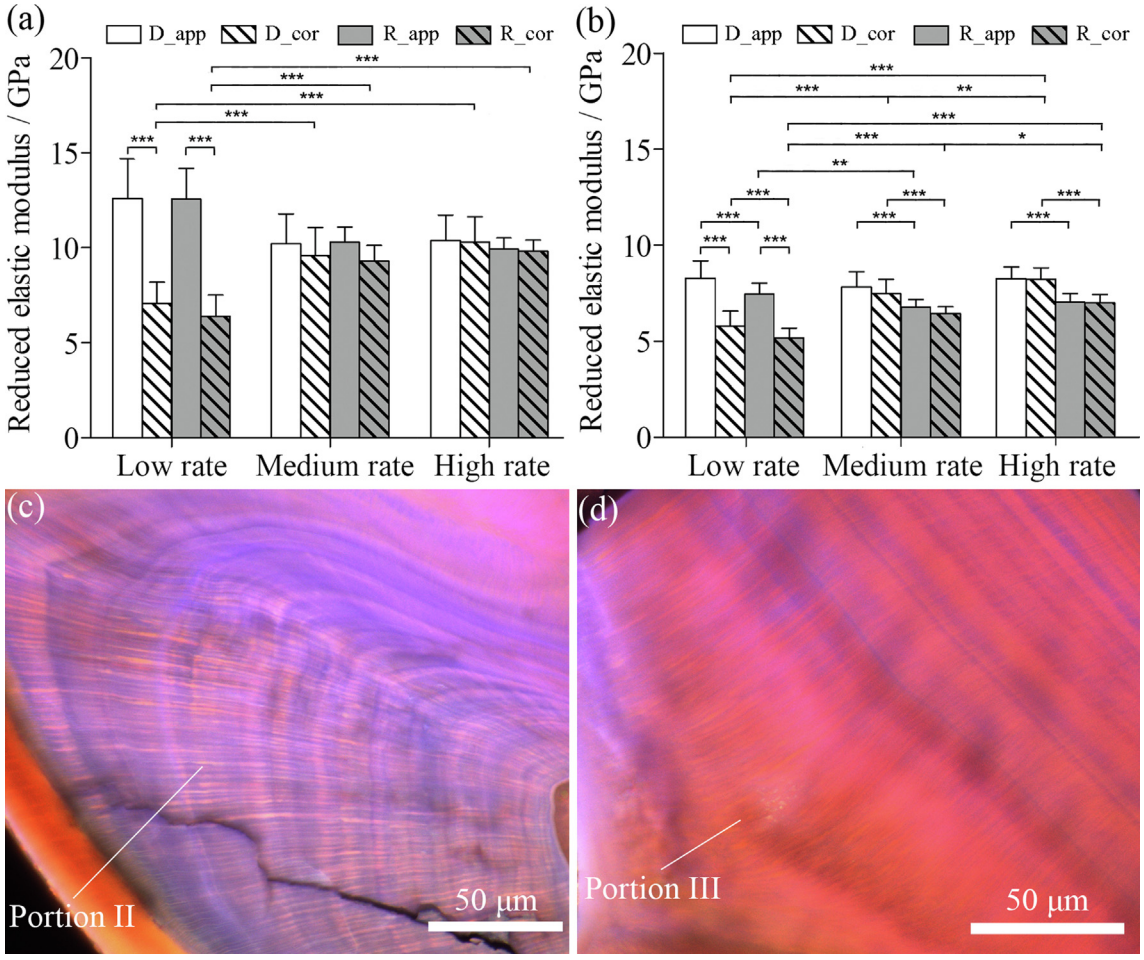

Fig. 2. Mechanical and compositional properties for the SLP portions II and III: the mechanical properties of portion II (a) and portion III (b) under different strain rates; the cross-sectional images of portion II (c) and portion III (d) under CLSM. The low, medium, and high strain rates correspond to 0.0083, 0.083, and 0.83/s, respectively. The red autofluorescence under CLSM represents chitin while the blue autofluorescence represents resilin proteins. D_app: $E_{r,app}$ for dry samples; D_cor: $E_{r,cor}$ for dry samples; R_app: $E_{r,app}$ for rewetted samples; R_cor: $E_{r,cor}$ for rewetted samples. *: P < 0.05; **: P < 0.01; ***: P < 0.001. (For interpretation of the references to color in this figure legend, the reader is referred to the web version of this article.)

Table 1
The efficiency ratio results of elastic energy storage ($\Re$) in the SLP portions under different conditions (Unit: %).

	Low rate	Medium rate	High rate
Dry portion II	56 ± 5.9	94 ± 1.2	99 ± 0.54
Rewetted portion II	51 ± 6.8	90 ± 1.9	99 ± 0.37
Dry portion III	70 ± 4.4	95 ± 0.62	99 ± 0.064
Rewetted portion III	69 ± 6.0	95 ± 1.0	99 ± 0.089

Note: Mean ± SD (n = 18).

amount of energy loss for the rewetted portions under the low strain rate mainly results from the creep dissipation of hydrated resilin component. Because of its higher resilin proportion, the rewetted portion II has a distinctly lower efficiency ratio under the low and medium rates than the rewetted portion III. Similarly, the dry portion II is significantly less efficient in energy storage than the dry portion III under the low strain rate (56 ± 5.9% vs. 70 ± 4.4%), which might also be attributed to the resilin component. Compared to hydrated resilin, dry resilin is more brittle and apt to crack under loading (King, 2010). The higher resilin amount of the dry portion II leads to more energy dissipation caused by the resilin breakage as well as frictions on the potential interfaces between fractured resilin components.

Despite the lower efficiency of elastic energy storage in the SLP portions, locusts also adopt other strategies to solve the conflict between power amplification and energy dissipation. Given the duration measurements of locust movements and the corresponding strains in the deformed SLP (Bennet-Clark, 1975; Burrows and Morris, 2001; Wan et al., 2016), the averaged strain rate for portions II and III were 0.02/s and 0.04/s in energy storage and 0.6/s and 1.0/s in energy release for jumping, 0.03/s and 0.04/s in energy storage and 5.0/s and 6.6/s in energy release for kicking, respectively. The physiological strain rates for these rapid movements are somewhat higher than the low strain rate used in this study (i.e., 0.0083/s), meaning that locusts can avoid potential energy dissipation by elevating the loading speed during the energy storage stage. This finding further contributes to the optimization of actuator parameters for power amplification mechanisms in jumping robots.

In addition, our experiments show that regardless of water condition the $E_{r,cor}$ value of portion II increases significantly (P < 0.001 from ANOVA and post-hoc) as the strain rate increases from 0.008/s to 0.08/s, but it tapers off as the strain rate increases further. On the contrary, the $E_{r,cor}$ value of portion III shows a significant increase with the strain rates under both the dry and rewet conditions. The result deviates from the rate-independent elastic modulus of the tarsal cuticle of bed bugs (Bustamante et al., 2017). This is because the mechanical properties of these cuticle samples are anisotropic, and the two tests have been conducted along two different directions. We measured the mechanical

properties along the femoral longitudinal axis of the SLP cuticle, while Bustamante et al. (2017) measured those in the normal direction of the tarsal cuticle. Furthermore, we have obtained the Young's modulus of the two SLP portions in the range of 4.1–8.2 GPa (with Poisson's ratio being assumed as 0.45), which is close to the results of tibia and wing cuticles reported by Vincent and Wegst (2004).

Finally, we find that both the apparent and corrected moduli of portion III are significantly reduced by water under all strain rates ($P < 0.001$ from *t*-test) while the variation in the mechanical properties of portion II with different water contents is insignificant. These results of portion II show a deviation from those of some other locust cuticles (Schöberl and Jäger, 2006; Klocke and Schmitz, 2011). This might be due to the difference of their microstructures: the SLP portion II has well aligned microfibers, while the sternal plates (Klocke and Schmitz, 2011) and the mandible cuticles of locust (Schöberl and Jäger, 2006) have greatly different microstructures. It is indicative that the regular arrangement of chitin microfibers may compensate the softening effect of water content on the elastic modulus of the SLP portion II.

Declaration of Competing Interest

The authors declare that they have no conflict of interest associated with the presented work.

Acknowledgments

The authors thank for the help of Mrs. Ming Qiang and Dr. Huijie Leng of Peking University. This work was supported by Beijing Natural Science Foundation (for C.W.; 3174051), Beijing Institute of Technology Research Fund Program for Young Scholars (for C. W.; 3052019066), the State Key Laboratory of Tribology (for Z.H.; SKLT2018B07), and the National Natural Science Foundation of China (for X.F.; 11432008).

Appendix A. Supplementary material

Supplementary data to this article can be found online at https://doi.org/10.1016/j.jbiomech.2019.08.008.

References

Bennet-Clark, H.C., 1975. The energetics of the jump of the locust schistocerca gregaria. J. Exp. Biol. 63, 53–83.
Burrows, M., Sutton, G.P., 2012. Locusts use a composite of resilin and hard cuticle as an energy store for jumping and kicking. J. Exp. Biol. 215, 3501–3512.
Burrows, M., Morris, G., 2001. The kinematics and neural control of high-speed kicking movements in the locust. J. Exp. Biol. 204, 3471–3481.
Bustamante, J., Panzarino, J.F., Rupert, T.J., Loudon, C., 2017. Forces to pierce cuticle of tarsi and material properties determined by nanoindentation: the Achilles heel of bed bugs. Biol. Open 6, 1541–1551.
Chamis, C.C., 1989. Mechanics of composite materials: past, present and future. ASTM J. Compos. Technol. Res. 11, 3–14.
Chen, P.Y., Lin, A.Y., McKittrick, J., Meyers, M.A., 2008. Structure and mechanical properties of crab exoskeletons. Acta Biomater. 4, 587–596.
Dirks, J.-H., Parle, E., Taylor, D., 2013. Fatigue of insect cuticle. J. Exp. Biol. 216, 1924–1927.
Hay, J.C., Bolshakov, A., Pharr, G.M., 1999. A critical examination of the fundamental relations used in the analysis of nanoindentation data. J. Mater. Res. 14, 2296–2305.
Klocke, D., Schmitz, H., 2011. Water as a major modulator of the mechanical properties of insect cuticle. Acta Biomater. 7, 2935–2942.
King, R.J., 2010. Dynamic Mechanical Properties of Resilin Master Thesis. Virginia Polytechnic Institute and State University, Blackburg.
Maier, V., Durst, K., Mueller, J., Backes, B., Höppel, H.W., Göken, M., 2011. Nanoindentation strain-rate jump tests for determining the local strain-rate sensitivity in nanocrystalline Ni and ultrafine-grained Al. J. Mater. Res. 26, 1421–1430.
Michels, J., Gorb, S.N., 2012. Detailed three-dimensional visualization of resilin in the exoskeleton of arthropods using confocal laser scanning microscopy. J. Microsc. 245, 1–16.
Ngan, A.H.W., Wang, H.T., Tang, B., Sze, K.Y., 2005. Correcting power-law viscoelastic effects in elastic modulus measurement using depth-sensing indentation. Int. J. Solids Struct. 42, 1831–1846.
Oliver, W.C., Pharr, G.M., 1992. An improved technique for determining hardness and elastic-modulus using load and displacement sensing indentation experiments. J. Mater. Res. 7, 1564–1583.
Patek, S.N., Dudek, D.M., Rosario, M.V., 2011. From bouncy legs to poisoned arrows: elastic movements in invertebrates. J. Exp. Biol. 214, 1973–1980.
Peisker, H., Michels, J., Gorb, S.N., 2013. Evidence for a material gradient in the adhesive tarsal setae of the ladybird beetle Coccinella septempunctata. Nat. Commun. 4, 1661.
Pharr, G.M., Oliver, W.C., Brotzen, F.R., 1992. On the generality of the relationship among contact stiffness, contact area, and elastic-modulus during indentation. J. Mater. Res. 7, 613–617.
Rajabi, H., Shafiei, A., Arvizeh, A., Dirks, J.-H., Appel, E., Gorb, S.N., 2016. Effect of microstructure on the mechanical and damping behaviour of dragonfly wing veins. R. Soc. Open Sci. 3, 160006.
Schöberl, T., Jäger, I.L., 2006. Wet or dry – hardness, stiffness and wear resistance of biological materials on the micron scale. Adv. Eng. Mater. 8, 1164–1169.
Tang, B., Ngan, A.H.W., 2003. Accurate measurement of tip-sample contact size during nanoindentation of viscoelastic materials. J. Mater. Res. 18, 1141–1148.
Vincent, J.F.V., Wegst, U.G.K., 2004. Design and mechanical properites of insect cuticle. Arthropod Struct. Devel. 33, 187–199.
Wan, C., Hao, Z.X., Feng, X.-Q., 2016. Structures, properties, and energy-storage mechanisms of the semi-lunar process cuticles in locusts. Sci. Rep. 6, 35219.
Zhao, Z.L., Shu, T., Feng, X.-Q., 2016. Study of biomechanical, anatomical, and physiological properties of scorpion stingers for developing biomimetic materials. Mater. Sci. Eng. C 58, 1112–1121.